RSC Advances

ROYAL SOCIETY OF CHEMISTRY

www.rsc.org/advances

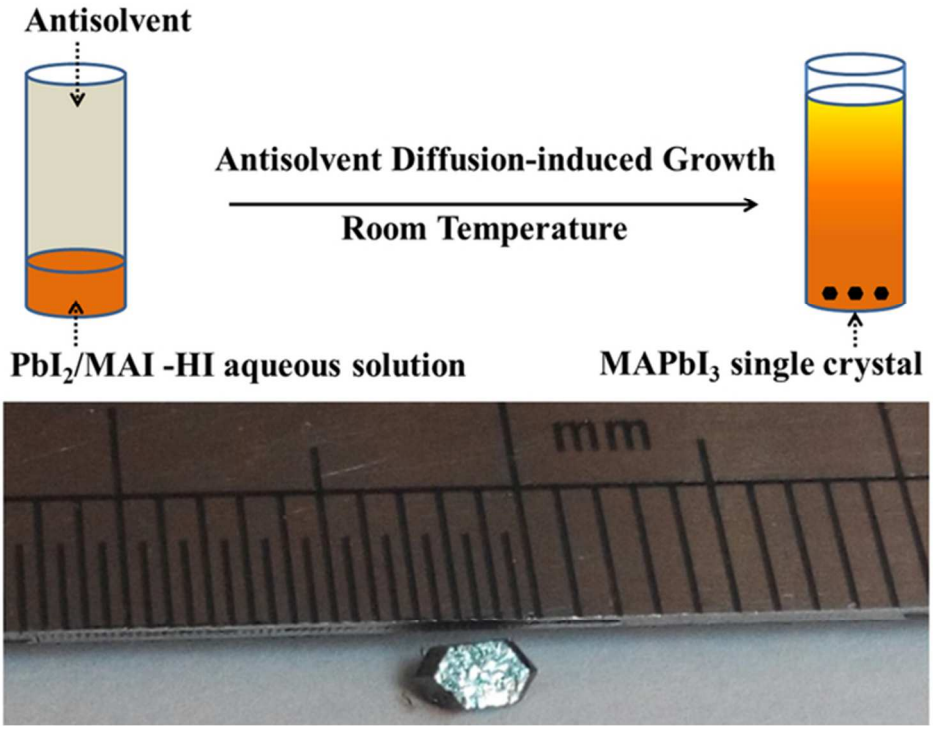

Antisolvent diffusion-induced growth, equilibrium behaviours in aqueous solution and optical properties of CH3NH3PbI3 single crystals
58x43mm (300 x 300 DPI)

Cite this: DOI: 10.1039/c0xx00000x

www.rsc.org/xxxxxx

ARTICLE TYPE

Antisolvent Diffusion-induced Growth, Equilibrium Behaviours in Aqueous Solution and Optical Properties of $CH_3NH_3PbI_3$ Single Crystals for Photovoltaic Applications

Huawei Zhou[a], Zhonghao Nie[a], Jie Yin[b], Yuanwei Sun[a], Hongyan Zhuo[a], Da-qi Wang[a], Dacheng Li[a], Jianmin Dou[a], Xianxi Zhang[a*], Tingli Ma[c]

Received (in XXX, XXX) Xth XXXXXXXXX 20XX, Accepted Xth XXXXXXXXX 20XX
DOI: 10.1039/b000000x

Crystallization and decomposition of organolead trihalide perovskites (OTPs) are very sensitive to the presence of water in precursor or in ambient conditions. Thus, understanding equilibrium behaviours (crystallization and decomposition) of OTPs in aqueous solution is very critical for OTP solar cell fabricated with water-based precursor solution. Here, equilibrium behaviours in aqueous solution of $CH_3NH_3PbI_3$ ($MAPbI_3$) single crystals (MSCs) were studied. Diethyl ether, as an antisolvent, effectively diffused and induced MSC growth by screening different solvents (diethyl ether, tetrahydrofuran, dichloromethane, and chloroform). The structure transform from initial PbI_2 to intermediate ($H_xPbI_{2+x}\,xH_2O$) and finally MSCs was observed by X-ray diffraction. Decomposition of MSCs in aqueous solution was significantly enhanced by potassium iodide coordination and inhibited by CH_3NH_3I (MAI) addition. We ascribed this inhibition behaviour to suppressing MAI migration from the MSC crystal structure. Finally, the optical properties of MSC were studied.

Introduction

Organolead trihalide perovskites (OTPs) process tunable band gap,[1, 2] high charge carrier mobility,[3] and long electron-hole diffusion.[4] With the continuous efforts from researchers worldwide, the power conversion efficiency of photovoltaic (PV) cells based on OTPs have been updated to 20.1%.[5] Moreover, one of the most attractive features for OTPs is that the high-performance device can be made with low-cost solution processing. However, solution-processed OTP thin films often encounter non-uniformity and incomplete coverage.[6] Consequently, understanding and controlling the crystallization process in solution processing is meaningful and has become one of the priorities of OTP-based scientists and manufacturers. The surface coverage of $CH_3NH_3PbI_3$ ($MAPbI_3$) is reduced by single-step spin-coating using a mixed solution of PbI_2 and CH_3NH_3I (MAI) in γ-butyrolactone (GBL) or N,N-dimethylformamide (DMF) solvent.[7] The use of CH_3NH_3Cl (MACl) precursor can slow down the crystallization process of $MAPbI_3$, thereby improving film morphology and extending the carrier's lifespan.[8–10] The precursor solubility or crystallization is controlled by 1,8-diiodooctane,[11] HI,[1] dimethyl sulfoxide (DMSO) solvent additive,[12] or solvent[13] for highly uniform and dense perovskite layers. Meanwhile, exposure of $MAPbI_3$ precursor films to chlorobenzene,[14] dichlorobenzene, DMSO,[15] toluene,[12] diethyl ether,[16] and DMF[17] can be an alternative approach to facilitate the crystallization or recrystallization of perovskites. Recently, Wang et al. developed a new precursor, $HPbI_3$, which enables crystallization of highly uniform formamidium lead iodide ($FAPbI_3$) films through a one-step spin-coating process.[18]

Besides the solution chemical of OTP polycrystal film, solution-grown $MAPbI_3$ single crystal (MSC) is beneficial to accurately understand their intrinsic physical, chemical, and optoelectronic properties. OTP single crystal is grown by cooling-induced crystallization, which may cause different crystal phases arising from the temperature-dependent phase transitions in OTPs.[3, 4, 19] Recently, mild heating of $CH_3NH_3PbBr_3$ DMF solution at about 50 ℃ will form red single crystals after several hours without solvent evaporation.[20] Kadro et al. presented a facile method for the growth of freestanding crystals of $MAPbI_3$ from GBL solution using inverse solubility at high temperatures.[21] Almost at the same time, Saidaminov et al. also reported the growth of shape-controlled OTP single crystal by inverse temperature crystallization.[22] Shi et al. reported an antisolvent vapor-assisted [dichloromethane (DCM)] crystallization approach to create $MAPbX_3$ single crystals.[21] Although the idea of antisolvent vapor diffusion induced crystallization methods in organic solvent DMF for OTP single crystal have been reported, crystallization and decomposition of OTP single crystal in aqueous solution are still unclear.

In this work, our study is focus on antisolvent diffusion-induced growth, and equilibrium behaviours in aqueous solution of OTP single crystal. MSCs were synthesized in MAI and $H_xPbI_{2+x}\,xH_2O$ precursor by antisolvent diffusion-induced (ASDI) method at room temperature. The structure transform from initial

PbI_2 in HI aqueous solution to finally MSCs was investigated by X-ray diffraction (XRD). On the other hand, decomposition of MSCs in aqueous solution was significantly enhanced by potassium iodide addition, and inhibited by CH_3NH_3I addition. We ascribed this inhibition behavious to suppressing MAI migration from the MSC crystal structure. Finally, the optical properties of MSC were studied.

Experimental Section

Synthesis of CH_3NH_3I: CH_3NH_3I were synthesized from 10 mL hydroiodic acid (57% wt.%, in water, J&K Chemical), by reacting 27 mL methylamine (40% in methanol, Sigma) in a 250-mL roundbottomed flask at 0 ℃ for 2 h with stirring. The precipitates were recovered by evaporating the solutions at 50 ℃. The products were dissolved in ethanol, recrystallized using diethyl ether, and finally dried at 60 ℃ in a vacuum oven for 24 h. The phase purity of the sample was confirmed by NMR as shown in Figure S2 [1H NMR (d6-DMSO) δ 7.51 (br s, 3H,$CH_3\underline{NH_3}^+I^-$), 2.38 (s, 3H,$\underline{CH_3}NH_3^+I^-$)].

Antisolvent Diffusion-induced Growth (ASDI) of $CH_3NH_3PbI_3$ Single Crystals: In a typical procedure, A 50 ml round bottom flask was charged with HI (1.82 ml, HI 55% wt.%, 0.023 mmol, in water, Energy). The liquid was degassed by passing a stream of nitrogen through it for 1 min and keeping it under a nitrogen atmosphere throughout the experiment. PbI_2 (115 mg, 0.25 mmol) was dissolved in HI solution upon heating the flask to 120°C using an oil bath, forming a bright yellow solution. To the hot yellow solution was added solid CH_3NH_3I (40 mg, 0.25 mmol) dissolving immediately. The stirring was discontinued and the solution was left to cool back to room temperature. The solution was transferred to cuvette. Antisolvent inflow into cuvette very slowly along cuvette wall. The cuvette was left to grow single crystal at room temperature without disturbance. The single crystal were washed by diethyl ether and dried in vacuum as raw materials for characterization.

Single crystal XRD Characterization:
Data was collected on a Bruker SMART 1000 CCD diffractometer with the use of Mo-*K*α radiation (λ = 0.71073 Å). The structures were solved by direct method and expanded with the use of difference Fourier techniques with the SHELXL-97 program.

$MAPbI_3$ Single Crystal Film Characterization:
Powders XRD measurements were obtained using PANalyticalX Pert diffractometer (Cu Kα radiation at λ = 1.54 Å) sampling at 2 ° min, 40 ekV and 100 mA. UV-vis absorption spectrum and diffuse reflectance spectrum was obtained using UV/Vis/NIR spectrometer (Perkinelmer, lambda, 750S). Steady-state photoluminescence was carried out on LS55 Luminescence Spectrometer (Perkin Elmer instrument).

Results and Discussions

To determine the antisolvent that can induce the growth of $MAPbI_3$ single crystal, we selected four solvents (diethyl ether, tetrahydrofuran, DCM, and chloroform). As described in the experimental section, four kinds of solvents inflowed into the perovskite precursors. The final volume ratio of inflowed solvent and perovskite precursors was about 10:1. As shown in Figure S1,

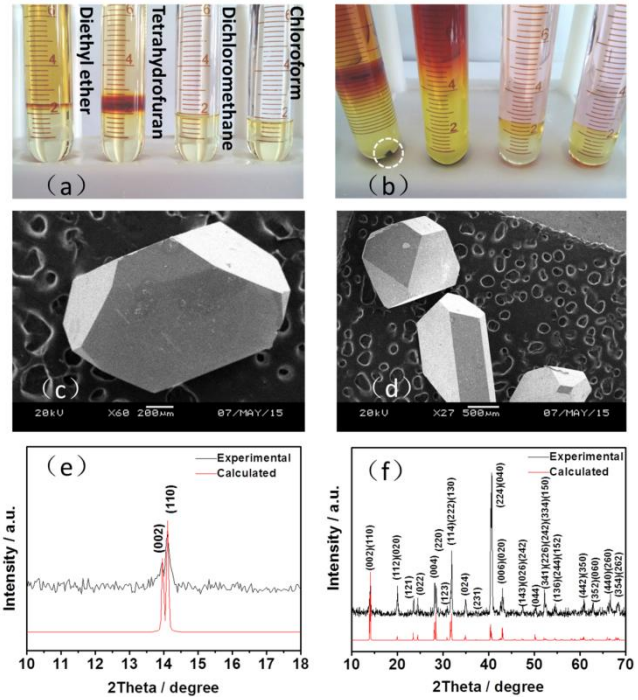

Figure 1. Crystal growth, SEM and diffraction. (a) Four solvent (diethyl ether, tetrahydrofuran, dichloromethane, chloroform) was inflowed into perovskite precursors. (b) Four solvent was inflowed into perovskite precursors after 2 days. SEM of $MAPbI_3$ single crystal formed in 0.1097 mol L^{-1} (c) and 0.1371 mol L^{-1} (d) PbI_2. Experimental and calculated powder XRD profiles of as-prepared $MAPbI_3$ single crystal at different arrange: (e) 10~18 °, (f)10~70 °.

the volume of perovskite precursors slightly increased when diethyl ether and tetrahydrofuran were inflowed, which indicated that diethyl ether and tetrahydrofuran diffused into the perovskite precursors. However, the volume of the perovskite precursors with methylene chloride or chloroform did not increase. $MAPbI_3$ single crystal was observed after 2 days with diethyl ether as antisolvent, whereas single crystals in other solvents were not observed (Figure 1 a, b). The basic idea of ASDI crystallization is the elegant combination of two miscible solvents. However, for dichloromethane and chloroform, neither of them are miscible with the water-based precursor solution, as shown in Figure 1 a, b. They hardly diffused into the water-based precursor solution and hardly increased the saturation of the perovskite precursors. Thus, dichloromethane and chloroform can not be regarded as antisolvent for ASDI crystallization in this study. For diethyl ether, it is miscible with the water-based precursor solution. The saturation of the perovskite precursors increased by diethyl ether diffusion, and the precursors showed gradual nuclear formation and growth to single crystals. Thus, diethyl ether is effective antisolvent to diffuse and induce MSC growth. Different concentration of perovskite precursors must affect the number of crystal nuclear and structure in the process of ASDI growth. When the concentration of perovskite precursors is 0.09595 mol L^{-1}, no single crystal was observed even after seven days. This concentration was too low to reach the sursaturation in the process of antisolvent diffusion. When the concentration increased to 0.1097 mol L^{-1} and 0.1371 mol L^{-1}, black single

crystals were observed after 2 days. From SEM (Figure 1c, d), we can see that single crystal processed high quality with crack-free, smooth surfaces, well-shaped borders. Single crystal X-ray diffraction (XRD) data (electronic supplementary information) showed that the as-grown crystals were attributed to $MAPbI_3$, which crystallizes in the tetragonal I4/mcm space group (a = b = 8.8719 Å, c = 12.6770 Å) in agreement with the previous results.[22] Detailed information of the single crystal is summarized in electronic supplementary information. The phase purity of the single crystals was confirmed by powder XRD from a large batch of crystals (Figures 1e and 2f). We found that the fit between the experimental patterns and calculated curves was good.

In order to study the transformation process in the single crystal growth in aqueous solution, we carried out XRD to study structure transformation. Compared to solubility of PbI_2 in H_2O, GBL or DMF, PbI_2 powder was easily dissolved in HI aqueous solution at room temperature, forming a bright yellow solution. This result indicated that coordination between PbI_2 and HI was formed, resulting in good solubility of PbI_2 in HI aqueous solution. In order to determine the structure of the coordination compound, the XRD characterization was carried out. For comparison, pure PbI_2 and PbI_2 dispersed in H_2O were also measured. As shown in Figure 2a, the diffraction peak of pure PbI_2 at 12.8 ° was attributed to (001) with a lattice spacing of 6.98 Å, indicating that a layered crystal structure of PbI_2, agreeing with literature.[23] Compared to pure PbI_2, the diffraction peaks at low angle of the powder obtained from PbI_2 dispersed in H_2O moved from 12.8 ° to 12.6 °, while other diffraction peaks from 16 ° to 70 ° was not obviously moved. This result indicated that the H_2O molecule inserted into the layered PbI_2 structure increased the lamellar distance following reaction (1).

$$PbI_2\ (s,\ yellow)+xH_2O\ (aq) \rightleftharpoons PbI_2{\cdot}xH_2O\ (s,\ yellow) \quad (1)$$

$$PbI_2\ (s,\ yellow)+xH_2O\ (aq)+xHI\ (aq) \rightleftharpoons H_xPbI_{2+x}{\cdot}xH_2O\ (aq) \quad (2)$$

$$H_xPbI_{2+x}{\cdot}xH_2O(aq)+MAI(aq) \underset{\text{Diffusion}}{\overset{\text{Diethyl ether}}{\rightleftharpoons}} MAPbI_3(s,\ black) \quad (3)$$

The XRD pattern of the coordination compound for PbI_2 in HI aqueous solution was different from that of pure PbI_2, which indicated that edge-sharing PbI_6 octahedral was changed by HI coordination. The moles of PbI_2 and HI in solution were 0.25 mol and 0.023 mol, so the formed coordination compound was not stoichiometry $HPbI_3$ but H_xPbI_{x+2}. Powder XRD of PbI_2 dissolved in aqueous HI also showed a diffraction peak at 12.6 °, indicating that the structure was also layered with H_2O. Thus, the composition of PbI_2 dissolved in aqueous HI might be H_xPbI_{2+x} xH_2O, as shown in reaction (2). Based on XRD analysis of MSC, the diffraction peaks of PbI_2 moved from 12.8 ° to 14.1 °, illustrating that the layered structure disappeared and converted into a three-dimensional $MAPbI_3$ single-crystal structure [reaction (3)].

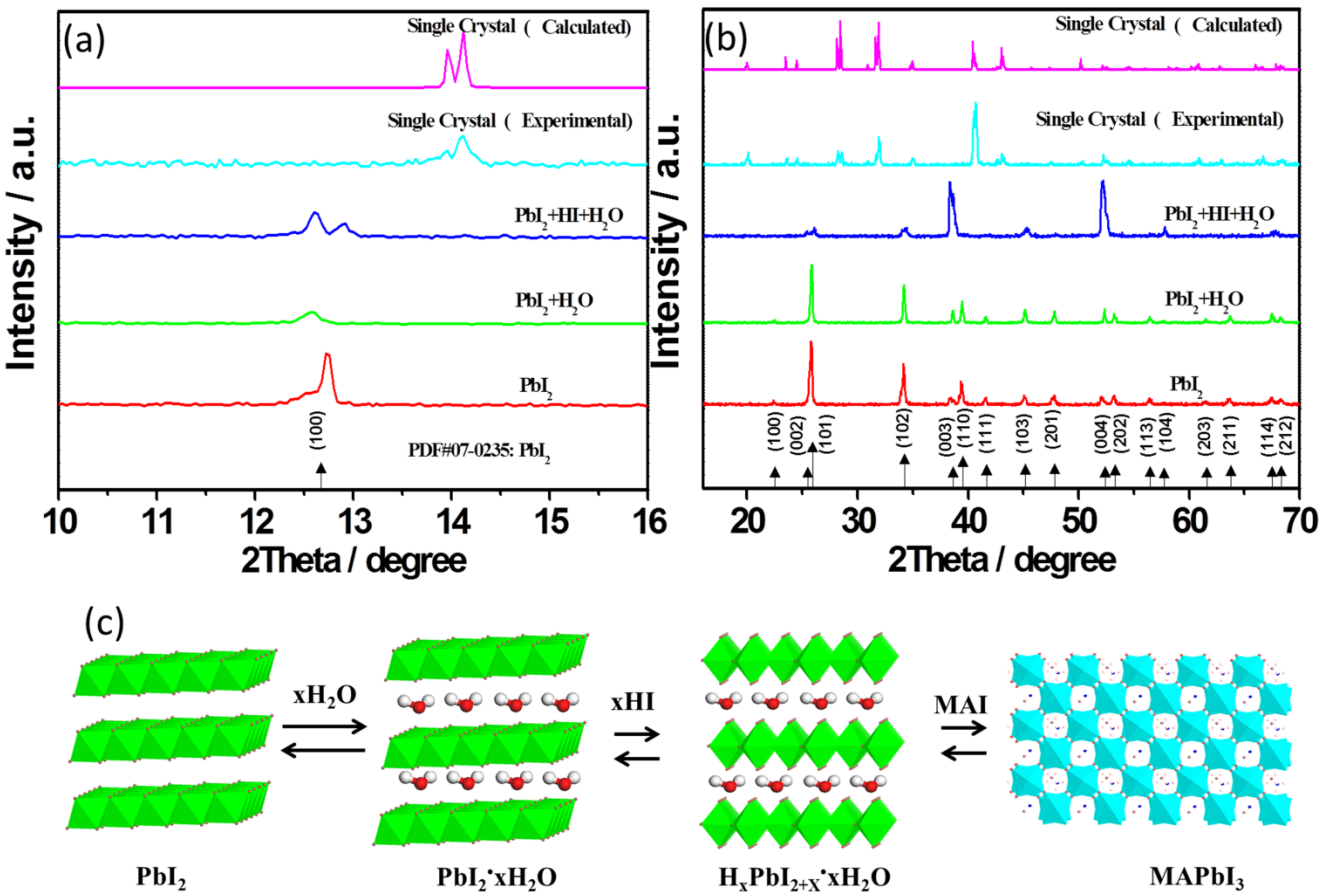

Figure 2. XRD patterns of PbI_2, PbI_2 in H_2O, PbI_2 in HI aqueous solution and MSC at different arrange.(a):10~20 °, (b)20~70 °. (c)Schematic illustration of the configurations of layered PbI_2 structue, PbI_2 xH_2O, H_xPbI_{2+x} xH_2O and $MAPbI_3$ single crystal.

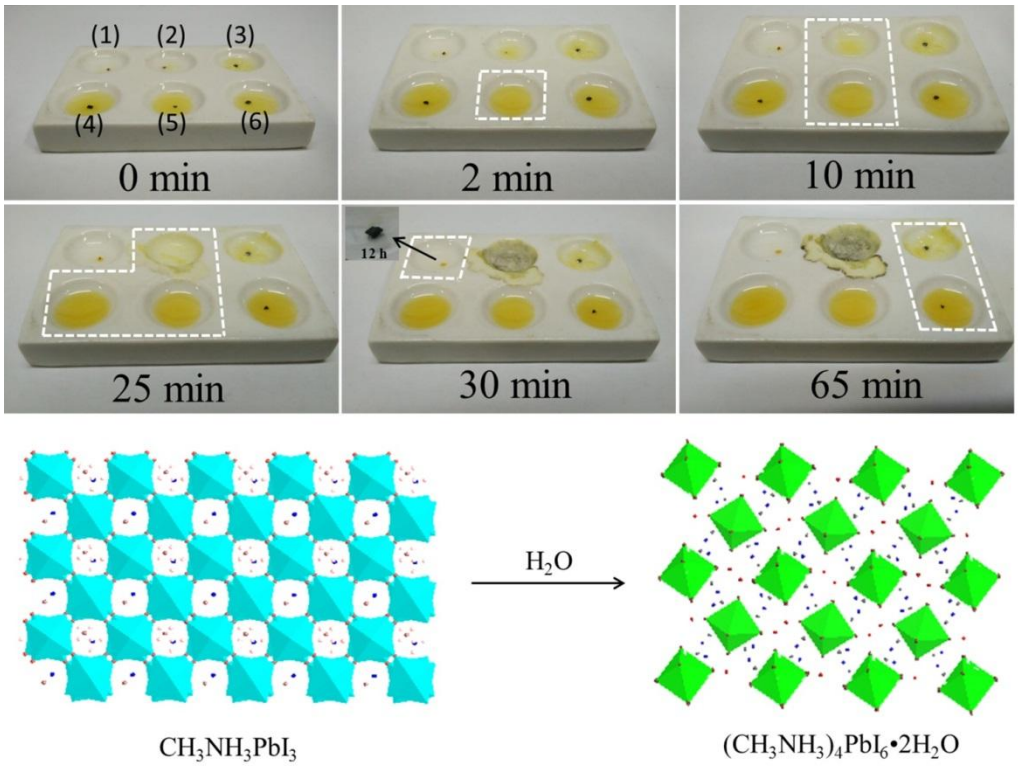

Figure 3. Photograph of the stability of $MAPbI_3$ single crystal in different solution at different time. (1) H_2O, (2) saturated KI aqueous solution, (3) saturated MAI aqueous solution, (4) 55% wt.% HI aqueous solution, (5) saturated KI in 55% wt.% HI aqueous solution, (6) saturated MAI in 55% wt.% HI aqueous solution. Schematic illustration of hydatation from $CH_3NH_3PbI_3$ to $(CH_3NH_3)_4PbI_6$ H_2O.

Understanding the decomposition of MSC in aqueous solution is helpful to solve the stability of MSC in the water. The decomposition of MSCs in different aqueous solutions, as shown in Figure 3, were analyzed. MSC in aqueous solution turned into yellow crystal rather than dissolving after 30 min. However，the yellow crystal recovered to black after 12 h (insert in Figure 3). This colour recovery phenomenon was also observed when polycrystal $MAPbI_3$ film were exposed to flow of 98 ± 2% relative humidity gas for a period of 24 h, and subsequently flushed with dry nitrogen gas (0% relative humidity).[23] Thus, the initial colour change from black to yellow of the MSCs decomposition process in aqueous solutions might be not an acid-base reaction of the methylammonium cation, but rather hydration of MSCs (as illustrated in Equation 4).

$$MAPbI_3(s, black)+H_2O(aq) \rightleftharpoons (CH_3NH_3)_4PbI_6{\cdot}2H_2O\ (s, yellow) \quad (4)$$

$$MAPbI_3(s, black)+xHI(aq) \rightleftharpoons MAI(aq)+H_xPbI_{2+x}\ (aq) \quad (5)$$

$$MAPbI_3(s, black)+xKI(aq) \rightleftharpoons MAI(aq)+K_xPbI_{2+X}\ (aq) \quad (6)$$

The MSCs in HI aqueous solution was dissolved after 25 min, as shown in reaction (5). Compared to solubility of MSC in HI aqueous solution, the MSCs in saturated KI aqueous solution and in saturated KI of HI aqueous solution were rapidly dissolved after 2 min and 10 min, respectively. Thus, KI promoted the dissolution of single crystal by coordination reaction (6). Interestingly, MSC could still be observed in saturated MAI aqueous solution or saturated MAI in HI aqueous solution after 65 min. These results indicated that excess MAI in solution could enhance the stability of MSC. The dominant reason might be that the massive MAI suppressed hydration of MSCs induced by hydrogen bond between MAI and H_2O molecule. Thus, in preparing OTPs solar cell process, massive MAI around OTP layer may enhance the stability of photovoltaic devices.

The thermal stability of the single crystal was measured by thermogravimetric analysis (Figure 4a). No apparent weight change was observed from 50 ℃ to 260 ℃. Although there is no obvious change in its quality, we can not determine whether the crystal phase of the perovskite crystal is changed. The weight of the single crystal began to reduce after 260 ℃, suggesting gradual degradation of the single crystal structure. Optical band gap (E_g) could be extrapolated method from diffuse reflectance spectrum (DRS) (Figure 4b) and the transformed Kubelka–Munk spectrum for the MSC film (Figure 4c). According to the Kubelka-Munk equation, the optical absorption coefficient F(R) can be expressed as $F(R)=(1-R)^2/2R$, where R is the percentage of reflected light. The relationship of the incident photon energy (hv) and E_g can be expressed as the transformed Kubelka-Munk function, $[F(R)hv]^p = A(hv - E_g)$, where E_g is the band gap energy, A is the absorption constant, h is the Planck' s constant, v is the frequency of the light (s^{-1}) and p is the power index that is related to the optical absorption process[24,25]. Theoretically p equals to 1/2 or 2 for an indirect or a direct allowed transition, respectively. According to literature, $MAPbI_3$ can be regard as direct allowed transition. Thus, E_g for the MSC film is determined to approximately 1.5 eV from the intercept of the

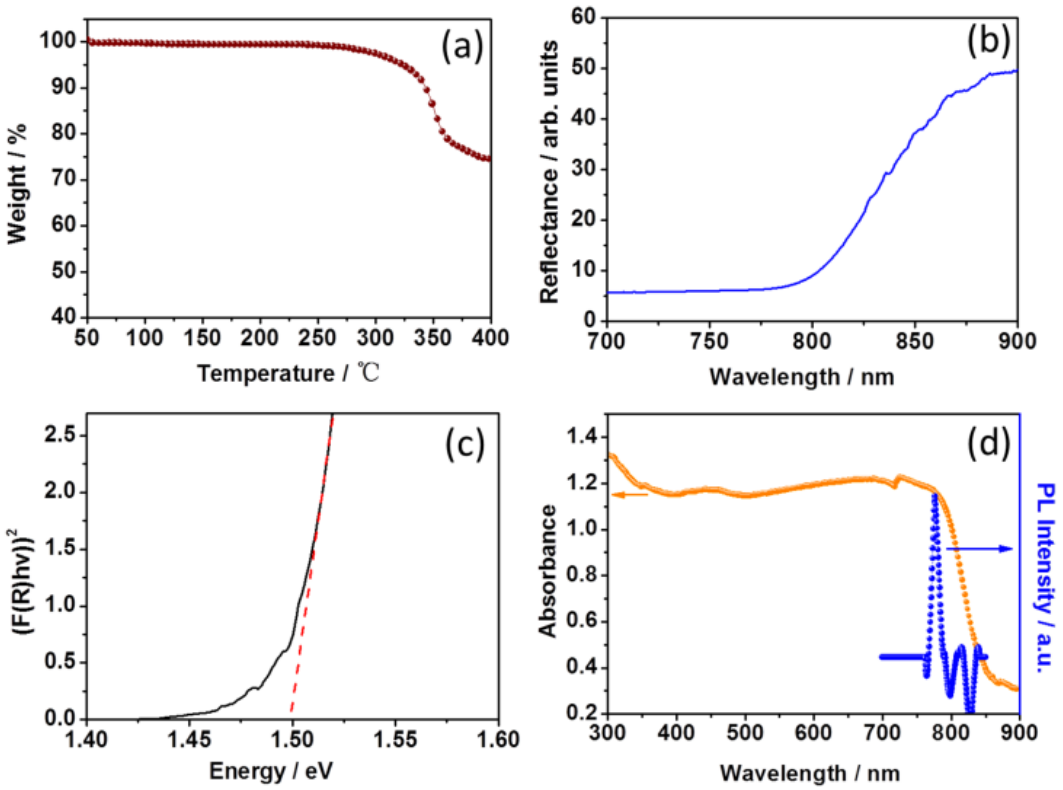

Figure 4. Thermogravimetric analysis and optical properties of $MAPbI_3$ single crystals: thermogravimetric analysis(a), diffuse reflectance spectrum (b), transformed Kubelka-Munk spectrum (c) and steady-state absorbance and photoluminescence (d).

liner part of $[F(R)hv]^2$ plot (Figure 4c) on the X axis. The MSC had a red-shift absorption band at 850 nm (Figure 4c), whereas regular polycrystal films had an absorption cut-off at 800 nm. This observation was consistent with the DRS results. The PL peak of the MSCs (776 nm) had a shorter wavelength than the absorption cut-off (Figure 4d). This overlap of the PL spectra with the absorption spectrum of MSC allowed photon recycling in thick MSC by reabsorbing the emission.

Conclusions

In summary, we have developed facile growth of $MAPbI_3$ single crystals by antisolvent diffusion-induced (ASDI) method at room temperature. Diethyl ether, as an antisolvent, can effectively diffuse and induce MSC growth. Compared to solubility of PbI_2 in H_2O, PbI_2 powder was easily dissolved in HI aqueous solution by coordination between PbI_2 and HI. The structure transform from initial layered PbI_2 to intermediate (H_xPbI_{2+x} xH_2O) and finally three-dimensional $MAPbI_3$ single crystal were observed. On the other hand, decomposition of $MAPbI_3$ single crystal in aqueous solution was significantly enhanced by potassium iodide coordination, and inhibited by CH_3NH_3I addition. We ascribed this inhibition behavious to suppressing MAI migration from the MSC crystal structure. These findings should be of interest to OTP-based scientists and manufacturers.

Acknowledgements

This work was financially supported by the National Basic Research Program of China (Grant No. 2011CBA00701), National High Technology Research and Development Program of China (Grant No. 2011AA050510), National Natural Science Foundation of China (Grant No.21171084), the Returned Overseas Researcher Foundation from the Ministry of Education, the Program for Scientific Research Innovation Team in Colleges and Universities of Shandong Province antae-Shan Scholar Research Fund.

Notes and references

[a]*Shandong Provincial Key Laboratory of Chemical Energy Storage and Novel Cell Technology, School of Chemistry and Chemical Engineering, Liaocheng University, Liaocheng 252059, China.*

[b]*College of Materials Science and Engineering, Liaocheng University, Liaocheng 252059, Shandong, China*

[c]*Graduate School of Life Science and Systems Engineering, Kyushu Institute of Technology, 2-4 Hibikino, Wakamatsu, Kitakyushu, Fukuoka 808-0196, Japan*

** Corresponding authors: zhangxianxi@lcu.edu.cn;*

Electronic Supplementary Information (ESI) available: Single crystal X-ray diffraction (XRD) data of $CH_3NH_3PbI_3$. Photograph of the crystallization process by antisolvent-diffusion induced method.e NMR of CH_3NH_3I. See DOI: 10.1039/b000000x/

1. G. E. Eperon, S. D. Stranks, C. Menelaou, M. B. Johnston, L. M. Herz and H. J. Snaith, *Energy Environ. Sci.*, 2014, **7**, 982-988.

2. J. H. Noh, S. H. Im, J. H. Heo, T. N. Mandal and S. I. Seok, *Nano Lett.*, 2013, **13**, 1764-1769.
3. C. C. Stoumpos, C. D. Malliakas and M. G. Kanatzidis, *Inorg. Chem.*, 2013, **52**, 9019-9038.
4. Q. Dong, Y. Fang, Y. Shao, P. Mulligan, J. Qiu, L. Cao and J. Huang, *Science*, 2015, **347**, 967-970.
5. W. S. Yang, J. H. Noh, N. J. Jeon, Y. C. Kim, S.Ryu, J. Seo, S. Seok, *Science*, 2015, DOI: 10.1126/science.aaa9272.
6. G. E. Eperon, V. M. Burlakov, P. Docampo, A. Goriely and H. J. Snaith, *Adv.Funct. Mater.*, 2014, **24**, 151-157.
7. J. Burschka, N. Pellet, S.-J. Moon, R. Humphry-Baker, P. Gao, M. K. Nazeeruddin and M. Graetzel, *Nature*, 2013, **499**, 316-320.
8. C. Wehrenfennig, G. E. Eperon, M. B. Johnston, H. J. Snaith and L. M. Herz, *Adv. Mater.*, 2014, **26**, 1584-1589.
9. N. Yantara, F. Yanan, C. Shi, H. A. Dewi, P. P. Boix, S. G. Mhaisalkar and N. Mathews, *Chem. Mater.*, 2015, **27**, 2309-2314.
10. P. Docampo, F. C. Hanusch, S. D. Stranks, M. Doeblinger, J. M. Feckl, M. Ehrensperger, N. K. Minar, M. B. Johnston, H. J. Snaith and T. Bein, *Adv. Energy Mater.*, 2014, DOI:10.1002/AENM.201400355
11. P.-W. Liang, C.-Y. Liao, C.-C. Chueh, F. Zuo, S. T. Williams, X.-K. Xin, J. Lin and A. K. Y. Jen, *Adv. Mater.*, 2014, **26**, 3748-3754.
12. N. J. Jeon, J. H. Noh, Y. C. Kim, W. S. Yang, S. Ryu and S. Il Seol, *Nat. Mater.*, 2014, **13**, 897-903.
13. Y. Wu, A. Islam, X. Yang, C. Qin, J. Liu, K. Zhang, W. Peng and L. Han, *Energy Environ. Sci.* 2014, **7**, 2934-2938.
14. M. Xiao, F. Huang, W. Huang, Y. Dkhissi, Y. Zhu, J. Etheridge, A. Gray-Weale, U. Bach, Y.-B. Cheng and L. Spiccia, *Angew. Chem.-Int. Edit.*, 2014, **53**, 9898-9903.
15. J. Lian, Q. Wang, Y. Yuan, Y. Shao and J. Huang, *J. Mater. Chem. A*, 2015, **3**, 9146-9151.
16. Y. Zhou, M. Yang, W. Wu, A. L. Vasiliev, K. Zhu and N. P. Padture, *J. Mater. Chem. A*, 2015, **3**, 8178-8184.
17. Z. Xiao, Q. Dong, C. Bi, Y. Shao, Y. Yuan and J. Huang, *Adv. Mater.*, 2014, **26**, 6503-6509.
18. F. Wang, H. Yu, H. Xu and N. Zhao, *Adv. Funct. Mater.*, 2015, **25**, 1120-1126.
19. T. Baikie, Y. Fang, J. M. Kadro, M. Schreyer, F. Wei, S. G. Mhaisalkar, M. Graetzel and T. J. White, *J. Mater. Chem. A*, 2013, **1**, 5628-5641.
20. T. Zhang, M. Yang, E. E. Bensonb, Z. Li, J. Lagemaat, J. M. Luther, Y. Yan, K. Zhu, Y. Zhao, Chem. Commun., 2015, **51**, 7820-7823.
21. J. M. Kadro, K. Nonomura, D. Gachet, M. Grätzel, A. Hagfeldt, *Sci. Rep.*, 2015, **5**, 11654.
22. M. I. Saidaminov, A. L. Abdelhady, B. Murali, Erkki Alarousu, V. M. Burlakov, W. Peng, I. Dursun, L. Wang, Y. He, G. Maculan, A. Goriely, T. Wu, O. F. Mohammed, O. M. Bakr, *Nat. Commun.* 2015, **6**, 7586.
23. D. Shi, V. Adinolfi, R. Comin, M. Yuan, E. Alarousu, A. Buin, Y. Chen, S. Hoogland, A. Rothenberger, K. Katsiev, Y. Losovyj, X. Zhang, P. A. Dowben, O. F. Mohammed, E. H. Sargent and O. M. Bakr, *Science*, 2015, **347**, 519-522.
24. X. Liu, S. T. Ha, Q. Zhang, M. de la Mata, C. Magen, J. Arbiol, T. C. Sum, Q. Xiong, *Acs Nano* 2015, *9*, 687-695.
23. J. Yang, B. D. Siempelkamp, D. Liu, T. L. Kelly, *Acs Nano* 2015, *9*, 1955-1963.
25. H.-S. Kim, C.-R. Lee, J.-H. Im, K.-B. Lee, T. Moehl, A. Marchioro, S.-J. Moon, R. Humphry-Baker, J.-H. Yum, J. E. Moser, M. Graetzel and N.-G. Park, *Sci. Rep.*, 2012, **2**, 519.
26. H. Lin, C. P. Huang, W. Li, C. Ni, S. Ismat Shah, Yao-Hsuan Tseng, *Appl. Catal. B: Environ.*, 2006, **68**,1–11.

